XII International Conference on Textile Composites and Inflatable Structures
STRUCTURAL MEMBRANES 2025
R. Wüchner, A. K. Goldbach, R. Rossi and C. Lázaro (Eds)

EVALUATION OF EQUIVALENT MEMBRANE STIFFNESSES OF SINGLE-SET ROPE MESHES

Dorothea A. Drayer

Jakob Rope Systems
Dorfstrasse 34, 3555 Trubschachen, Switzerland
e-mail: dorothea.drayer@jakob.ch, web page: www.jakob.com

Key words: membrane structure, mesh, rope, rope mesh, tensile structure, Webnet

Summary. In contrast to typical orthotropic membranes or rope meshes, which consist of two distinct sets of ropes or fibers, there is a type of rope mesh, where only one set of quasi-parallel ropes is alternatingly interconnected and then stretched to form a mesh. A significant non-linearity in-plane, a strong interaction between X- and Y-direction, and frequent local bending (a loading type uncommon for ropes) is characteristic for this type of mesh. In this paper, it is shown how the mesh behavior translates into unique membrane properties.

1 INTRODUCTION

Single-set rope meshes, called Webnet by producer and distributor Jakob Rope Systems, have been used for more than 20 years now as a third-party-approved building product[1] used in various applications for examples as safety meshes or for zoo enclosures.

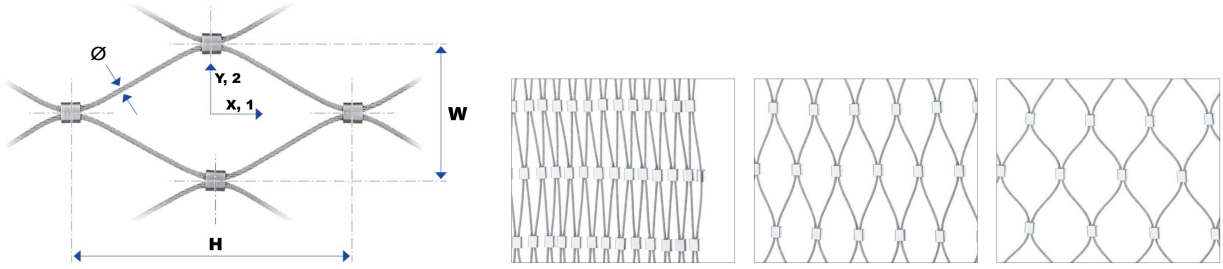

Figure 1: Geometry of a single mesh cell (left) and stretching process (right)

To perform engineering calculations, the corresponding material properties must be known. For large-scale structures, especially for free-form applications, global analysis of e.g. wind load scenarios and cutting pattern generation, the need arises to be able to formulate the Webnet as a surface with equivalent membrane stiffness. The advantage of a surface based input is that the mesh type can easily be changed by just changing the material properties and studying variants of form-finding with drastic perimeter rope deflection is streamlined.

For the Webnet various combinations of rope diameters (1 to 5 mm) and nominal mesh widths (20 to 400 mm) exist. Fig. 1 shows a typical mesh cell with the nominal opening angle of 60°.

The nominal pretension ratio following this opening angle is typically assumed to be p_x / p_y = 3/1.

The stiffness of conventional textile membranes is commonly obtained or verified by BIAX testing[2 3 4] Applying the same procedures to single-set meshes has been proven complex and tricky to evaluate[5]. Testing every combination of rope size, mesh type, mesh-cell-size, pretension and stretching-ratio is nearly impossible.

That means, that stiffness considerations must be based on general principles, which can be applied to all the various cell-sizes and mesh rope diameters. Further, it must be a quick usable approach for all-day engineering purposes, using existing software or spreadsheets. Compromises in accuracy are accepted, provided that the concept is robust and the critical points are known.

This paper is limited to the analysis of meshes with sleeves. Even though behavior and use-cases of "woven" sleeveless meshes can usually be considered equivalent to meshes with sleeves, there are some fine differences which aren't covered here. Even for the sleeves, different sleeve sizes exist: this is considered with the internal lengths of the model. The rope-sleeve connection is assumed fixed, internal sliding or failure analysis is not considered: all loads applied in this paper are to assess deformations only. Furthermore, this paper is dealing with normal stiffness. Shear stiffness is not covered in the scope of this paper.

2 BASICS

2.1 General formulation of membrane stiffness

The following equations are taken from literature[4], especially chapter 6.

The planar, linear-elastic, orthotropic material behavior, which is commonly used to describe membranes, is as follows:

$$\begin{bmatrix} n_{11} \\ n_{22} \\ n_{12} \end{bmatrix} = \begin{bmatrix} E_{1111} & E_{1122} & 0 \\ E_{2211} & E_{2222} & 0 \\ 0 & 0 & E_{1212} \end{bmatrix} \cdot \begin{bmatrix} \epsilon_{11} \\ \epsilon_{22} \\ \gamma_{12} \end{bmatrix} \tag{1}$$

This shows the relation between the stresses n, the strains ϵ and γ and the stiffness matrix $\mathbf{K}$, with its entries E_{1111}, E_{2222}, E_{1122} and E_{2211}.

Introduction of material constants allows us to reformulate as:

$$\begin{bmatrix} n_{11} \\ n_{22} \\ n_{12} \end{bmatrix} = \frac{1}{1-\nu_{12}\cdot\nu_{21}} \cdot \begin{bmatrix} E_1 & \nu_{12}\cdot E_2 & 0 \\ \nu_{21}\cdot E_1 & E_2 & 0 \\ 0 & 0 & (1-\nu_{12}\cdot\nu_{21})\cdot E_{1212} \end{bmatrix} \cdot \begin{bmatrix} \epsilon_{11} \\ \epsilon_{22} \\ \gamma_{12} \end{bmatrix} \tag{2}$$

By equating the matrix entries, the relation $E_{1111} = \frac{E_1}{1-\nu_{12}\cdot\nu_{21}}$ (and corresponding) can be formulated. By not taking sheer stiffness into consideration and transforming, Eq. 1 simplifies to:

$$\begin{aligned} n_{11} &= E_{1111}\cdot\epsilon_{11} + E_{1122}\cdot\epsilon_{22} \\ n_{22} &= E_{2211}\cdot\epsilon_{11} + E_{2222}\cdot\epsilon_{22} \end{aligned} \tag{3}$$

Symmetry is given by $E_{1122} = E_{2211}$. However, due to some effects in certain modeling / evaluation principles, both variables will be used in this paper.

The product $\nu_{12} \cdot \nu_{21}$ shall be called "Interaction value": it is apparent by the relation shown above, that this value must be < 1. Further, it is clear that $|\mathbf{K}| = E_{1111}E_{2222} - E_{1122}E_{2211}$ must be > 0 for **K** to be a valid, non-singular stiffness matrix.

2.2 The two basic hypotheses

In order to assess the membrane stiffness, two fundamentally different approaches have been developed.

- The **Beam-FEM-Approach** using beam elements with a realistic rope bending stiffness and a geometric non-linear calculation.
- The **Truss-Approach** using a very basic truss geometry to analytically asses the "as-installed" state.

If two fundamentally different approaches yield comparable results, then the behavior is well understood. Further there is the presupposition, that conclusions can be drawn about the entire mesh area based on the behavior of the individual mesh cell.

Different mesh configurations are considered: most common example in this paper is type "2-80", with the meaning of "cable diameter"-"nominal mesh width W" and both values in mm. For that type "2-80" the corresponding mesh height is H = 141 mm. This type is chosen due to its mid range for both mesh width and cable diameter. Corresponding heights for other widths (-40, -60, -120, -160) are given by the fixed ratio of W/H resp. the opening angle of 60°. Values for H can also be found in Tab. 5. The local coordinate systems X and Y resp. 1 and 2 always follows Fig. 1.

3 TESTING AND PREPARATORY BEAM-MODELING

3.1 Basic assumptions concerning FEM-Elements and modeling procedure

The rope is simplified as a common beam with the properties A, I $(Iy = Iz)$ and E. There is no modeling of the single wires. The **metallic section A** or A_m can be obtained with the fill factor f according to code[6]. Stainless steel 1.4401/AISI316 with a nominal wire tensile strength of $f_u = 1570 N/mm^2$ or 1 770 N/mm^2 is used as material for ropes.

The code further specifies a **Young modulus E** of stainless steel ropes as 90'000 (+/- 10'000) N/mm^2.[6] (Note: some literature refers to the rope Young modulus as "deformation modulus" or "secant modulus", because it is not a constant, natural material property.) For an in-house test of Ø3 6x19+WC with cast heads, maximum E did not exceed $70'000 N/mm^2$. Other experiments[7] show a similar behavior. There are thus four representative Young modulus, which are chosen to be considered further: $70'000 N/mm^2$ as a rounded up upper limit of the test, $90'000 N/mm^2$ of the code and $45'000 N/mm^2$ and $30'000 N/mm^2$ as half resp. third of the code value.

The planar **second moment of area I**, resp. the bending stiffness of a rope EI is not trivial due to its dependency on the load or stress, the internal friction, the rope construction and the curvature

of the rope[8 9]. There are considerations and empirical tests which cannot be addressed within the scope of this paper.

It is however possible, to easily calculate the theoretical minimum I_{min} and maximum I_{max} for the planar second moment of inertia for a rope[8], using fill factor f and the diameter of the single wires.

$$I_{min} = n_w \cdot \frac{{d_w}^4 \cdot \pi}{64} \tag{4}$$

$$I_{max} = f \cdot \frac{d^4 \cdot \pi}{64} \tag{5}$$

With the simplified assumption that each wire has the same diameter, the wire diameter d_w can be calculated using A_m and the number of wires n_w. The Tab. 1 gives an overview of used rope types and their section properties. The specified minimum breaking loads are based on $f_u = 1570N/mm^2$, but tensile strength is not relevant within the scope of this paper.

Table 1: Rope Types

$\emptyset[mm]$	$Type$	$f[-]$	$A_m[mm^2]$	n_w	$d_w[mm^2]$	$I_{max}[mm^4]$	$I_{min}[mm^4]$	$MBL[kN]$
1.5	6x7+WC	0.56	0.99	49	0.160	0.139	0.00159	1.37
2.0	6x7+WC	0.56	1.76	49	0.214	0.440	0.00503	2.40
3.0	6x19+WC	0.56	3.96	133	0.195	2.227	0.00938	4.60

Due to the experiments shown in[7], the $I_{effective}$ (resp. I) can be estimated to 1xI_{min} - 10xI_{min}, details will follow in the next section. For the second polar moment of area $J = 2 \cdot I_x$ resp. $J = 2 \cdot I_y$ is assumed, as for sections with rotational symmetry. Now with the values for A resp. the ranges for E and I, the Webnet can be modeled with beam elements.

As simplification, the initial state is modeled as parallel lines with a spacing of the rope diameter. The sleeve spacing along the ropes is mainly governed by the theoretical free rope length between the sleeves during production. The sleeve itself is modeled with four linear 1D-beam elements (simplified quadratic section with 1.5x1.5 mm), which form a rectangle.

Siemens NX Simcenter 3D is used (Version 1872) as software. The three tiered simulation procedure, starting with the parametrically controlled "part"-file defining the base grid of the sleeves and ropes, then meshing of the geometry in the "fem"-file (CBEAM elements, subtype PBEAM, element size 2mm) with finally solving in the "sim"-environment (nonlinear statics, large displacements enabled), shall only be mentioned here in passing.

3.2 Testing and modeling to verify bending stiffness

In order to gain insight into the transverse force-deformation behavior, tests were carried out on individual mesh cells, so that the actual values of E and I within the range of the min. and max. values explained in the previous chapter, can be more accurately assessed.

The test setup designed for this purpose has a fixed point for clamping one side of the mesh, a load application point for increasing the test load F and two clamps for applying the pretension P (each with weights and pulleys). The test specimen rests on a Teflon plate to reduce friction.

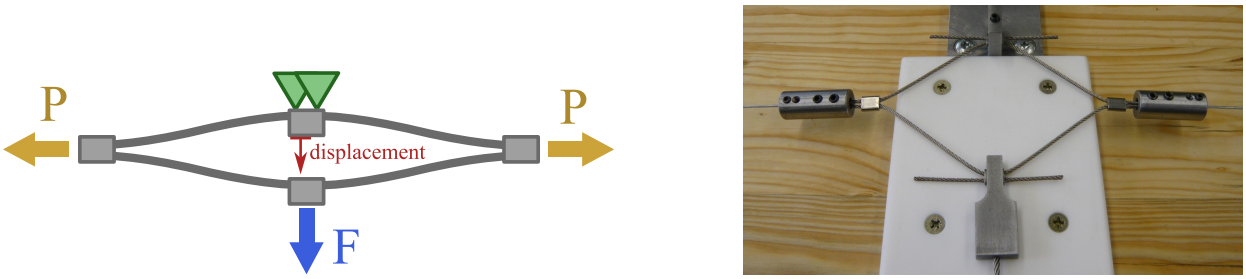

Figure 2: Testing schematics (left) and photo of the testing equipment (right)

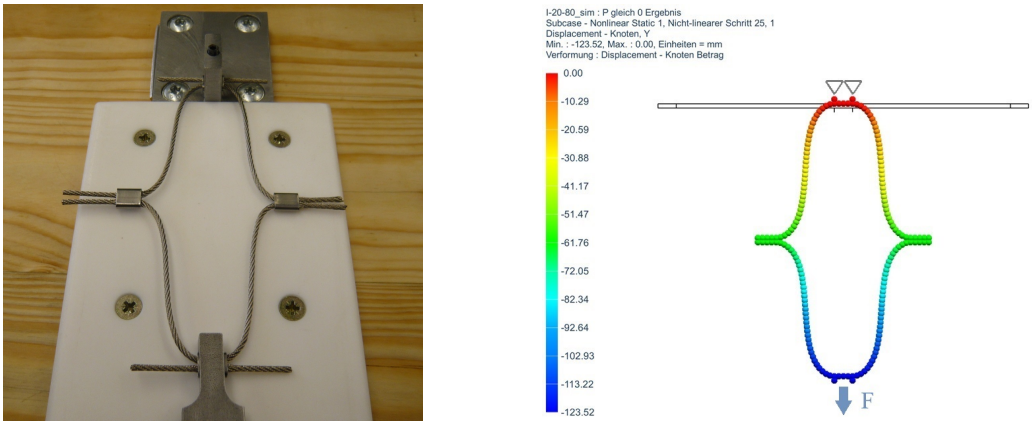

Figure 3: A testing load of F applied without pretension (left) and corresponding Beam-FEM-Modeling (right)

The tests were carried out by increasing the weights piece by piece (without unloading in between) and then measuring the distance with calipers. In the tests with pretension, the pretension weights were attached and kept constant throughout the test.

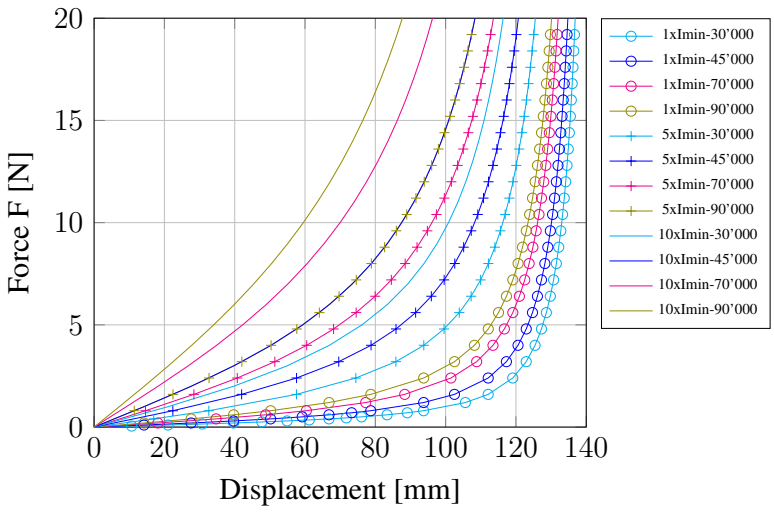

Figure 4: Modeling of 2-80 with varying bending stiffnesses

The unloading curve with its hysteresis is not subject of this paper. The test results, with comparison to FE modeling, can be found in Fig. 5 and 6. It should be noted, that the test results are only suitable for qualitative consideration, as the result values contain measurement inaccuracies, geometric tolerances of the samples and the influence of friction. Despite the generally uniform appearance, a certain degree of variation is visible for the tests.

The first step in modeling is a parameter study to verify the bending stiffness EI. Corresponding support condition as in Fig. 3 were assumed in the model. With the estimations made in the previous section, several force-displacement curves can be compared. I is specified as a multiple of I_{min} of Tab. 1 whereas the Young modulus is the 5-digit number (Fig. 4).

The curves for '5xI_{min}- 90'000' and '10xI_{min}- 45'000' are virtually identical, which shows that the bending stiffness is most relevant in that scenario and that the different tensile properties are not decisive.

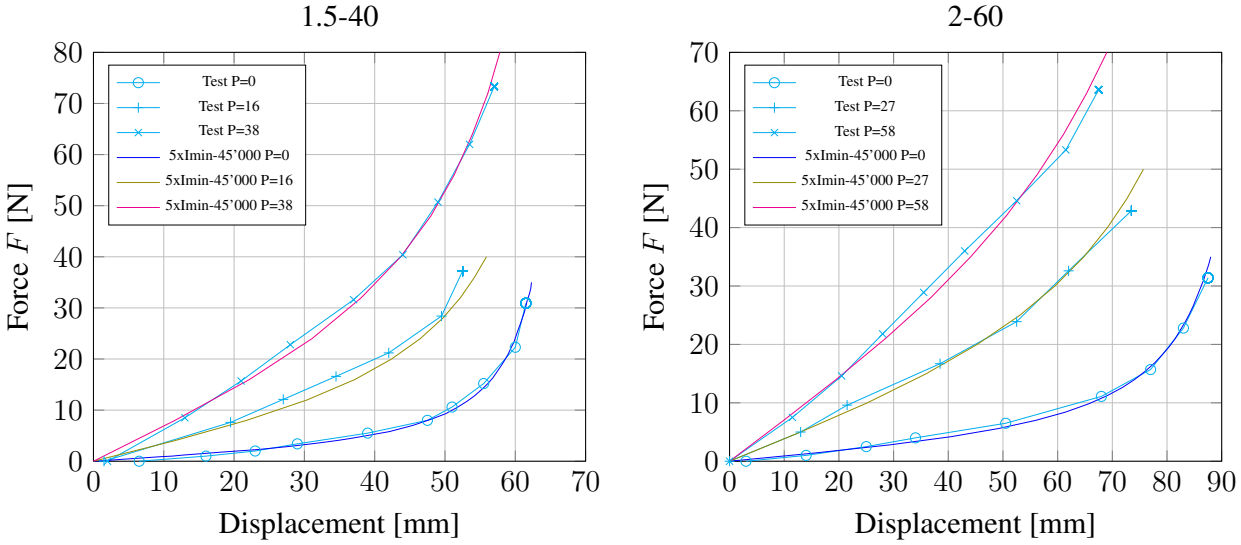

Figure 5: Simulation and tests 1.5-40 (left) und 2-60 (right)

The 5xI_{min} and $E = 45'000$ is a good fit for the test results, see the combined figure of 2-80 and other types. The strength of this approach is, that it does not only fit well for the initially regarded 2-80 without pretension, but also works well with pretension (P in [N]), the different mesh size 2-60 and even fits with 1.5-40 which is using a different rope diameter altogether.

For type 3-80, the 5xI_{min} is too stiff (gray line), however 4xI_{min} fits well, also with all tested pretension levels. This difference in I is likely due to the fact, that the ∅1.5 and ∅2 (both with 6x7+WC) have a different rope construction than ∅3 (6x19+WC)

All tests and models show, that the greater the pretension, the steeper the curve at the beginning, i.e. the greater the initial stiffness. For tests without pretension the curve is initially very flat and becomes increasingly steeper.

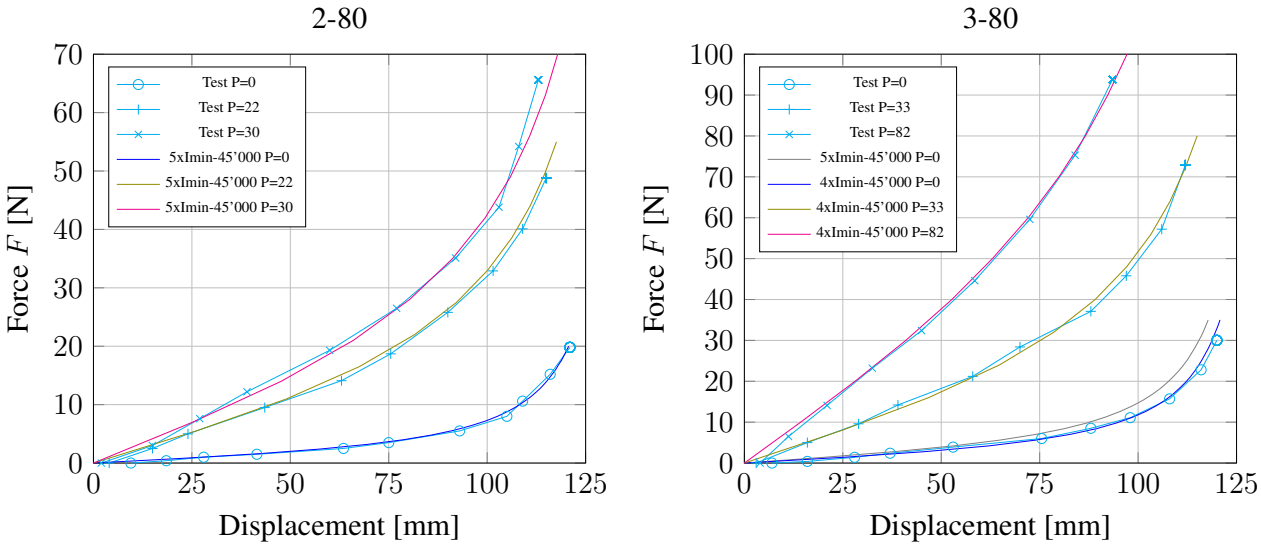

Figure 6: Simulation and tests 2-80 (left) und 3-80 (right)

3.3 Modeling of a single mesh cell loaded laterally

Now that the transverse load behavior of a single cell has been examined, the behavior while loaded laterally is analyzed further. The nominal mesh width is defined with a displacement of the support: the resulting shape is shown in Fig. 7 left. Then, a lateral force P_x is applied, and the displacement relative to the initial state is recorded. Both analyzed types (1.5-80 and 2-80) are modeled with the same effective sleeve length of 6 mm resp. same rope length to ensure comparability.

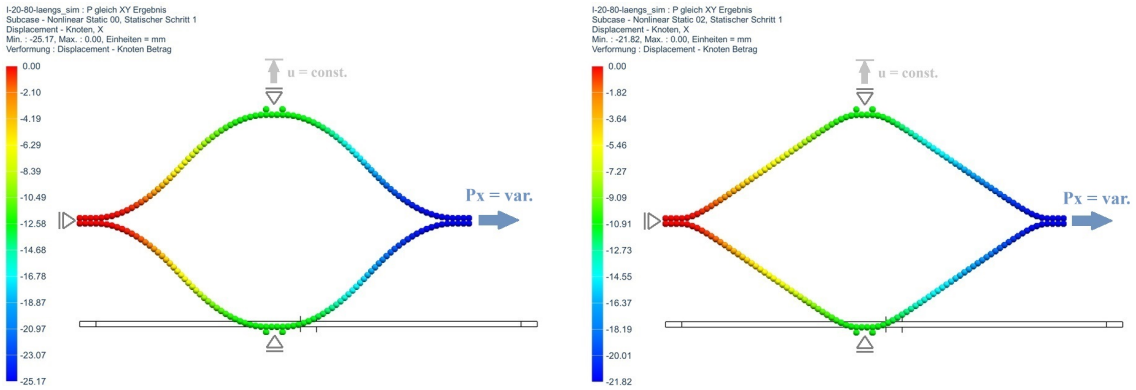

Figure 7: Lateral loading of 2-80 with initial state (left) and a tension P_x of 100 N (right)

The overall non-linearity Fig. 8 (left) can be roughly divided into three zones: the very soft initial behavior up to approx. 3mm, a considerably stiffer behavior starting at 4.5 mm and a transition zone in between. This stiffening behavior, the phenomena hereby called “S-bend-straightening”

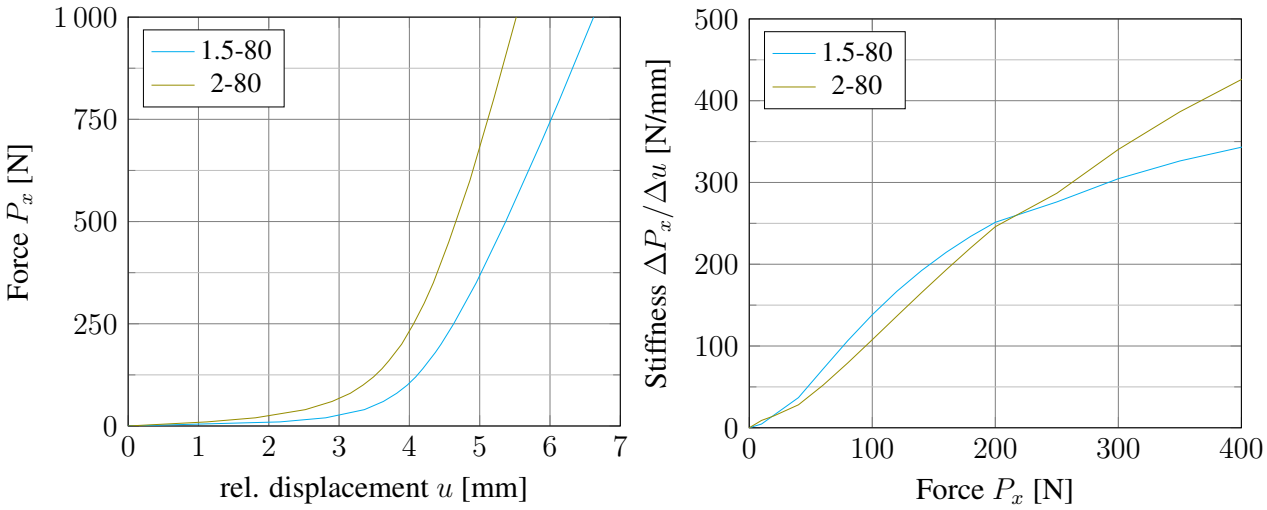

Figure 8: Simulation lateral: uniaxial behavior

is a fundamental characteristic of the mesh. Based on the load displacement curve, the linear equivalent spring-stiffness is calculated. A stiffness/load-diagram shows, that the smaller diameter behaves *stiffer* than the larger diameter up to approx 220 N. This issue is discussed and analyzed further in section 6.2.

3.4 Plausibility control by modeling out-of-plane loading

After transverse and lateral loading, also the out-of-plane-loading shall be calculated and compared with a test. This test was part of an in-house testing session to check the robustness of mesh configurations. The max. load of 10 kN was considerable, but did also not lead to tensile failure of any part of the 2-80.

Figure 9: Testing procedure (left) and Beam-FEM-Model (right) with an out-of-plane loading of approx 3000 N

With the additional loading type and the high maximum load, the results can give an indication about the quality or robustness of the previous assumptions of I=5xI_{min} and E=45′000 N/mm^2.

For this plausibility control, the load application in the model was simplified by distributing the total load over an approximate area (no disc or contact modeled), further the plastic deformability of the surrounding tubular perimeter frame was not included and the modeling support conditions were simplified (ideally sliding parallel to edge, ideally fixed in- and out-of-plane).

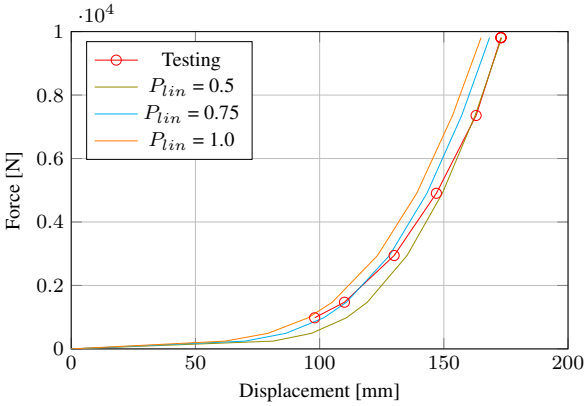

Figure 10: Out-of-plane loading

The exact linear mesh pretension in the experiment is not known, so 3 variants with P_{lin} of 0.5, 0.75 and 1.0 kN/m where analyzed. The three pretension levels form enveloping curves around the test data, which indicates that the mesh stiffness approach seems to be, at least in combination with the pretension approach, a suitable approximation. The softer behavior of the tests for high loads can be explained by the deformation of the tubular frame. Having the stiffness assumptions thus sufficiently verified, the modeling for the membrane stiffness can be performed.

4 BIAX-BEAM-FEM-MODELING

To obtain the membrane stiffness, the procedure illustrated in the European Design Guide[2] is modeled in a modified version to better suit the mesh behavior and to allow for apt evaluation. Furthermore, instead of time dependent curves with varying pretension rations, three distinct states are analyzed (Fig. 11)

Two different diameters (1.5 and 2) and five different mesh sizes per diameter where calculated. As materials parameters, the known A of 1.76 and 0.99 mm^2 where applied, beside the previously estimated I of 5xI_{min} and $E = 45'000 N/mm^2$.

For all mesh sizes and diameters a constant pretension per mesh cell is applied: $P_{x,state0} = 80N$, $P_{x,state1} = 160N$. (Which means however, that due to varying cell mesh sizes, the linear pretension varies.) State 0 and 1 both have the same path controlled displacement of the “upper” edge, which is defined by the nominal mesh width.

The normal forces in X- and Y-direction are then evaluated at the rectangle sleeve for convenient transformation to linear loads. By applying the resulting displacement u_x of state 0 to the right hand edge as a path-controlled bearing displacement, the geometry for state 2 is defined. The internal forces F_y of state 0 is doubled and applied as external loading for state 2. Strains are calculated with the resulting displacements and the known geometry of state 0.

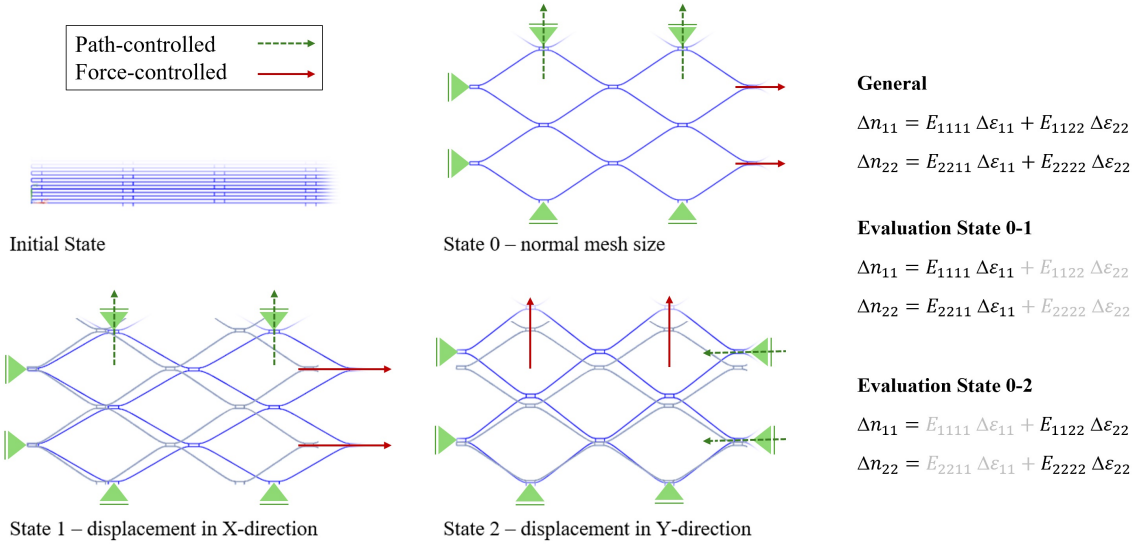

Figure 11: BIAX-Modeling

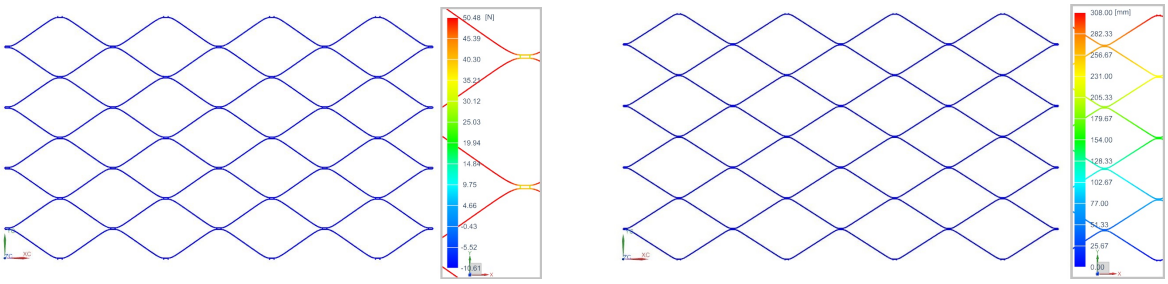

Figure 12: State 0 for type 2-80 with normal forces and state 0 for 1.5-80 with y-displacement

4.1 BIAX-Beam-FEM-Modeling of Ø1.5 and Ø2 meshes

The stress and strain results shall be given for one example, the 2-80:
Results state 0-1: $\Delta n_{11} = 1.00 kN/m$; $\Delta n_{22} = 0.35 kN/m$; $\Delta \epsilon_{11} = 0.0039$; $\Delta \epsilon_{22} = 0.0$
Results state 0-2: $\Delta n_{11} = 1.07 kN/m$; $\Delta n_{22} = 0.40 kN/m$; $\Delta \epsilon_{11} = 0.0$; $\Delta \epsilon_{22} = 0.0119$

With this, the stiffness matrix entries can be calculated. The complete set of results for both modeling series are given below.

The in-depth interpretation of these results will be done in section 6, the most notable points shall be mentioned here: E_{1111} is multiple times larger than E_{2222}, E_{1122} and E_{2211} are almost identical and also significantly larger than E_{2222}. For both diameters, the stiffness is reduced with increasing mesh size. Notable is, that the BIAX-stiffness for Ø1.5 is *higher* than for Ø2.

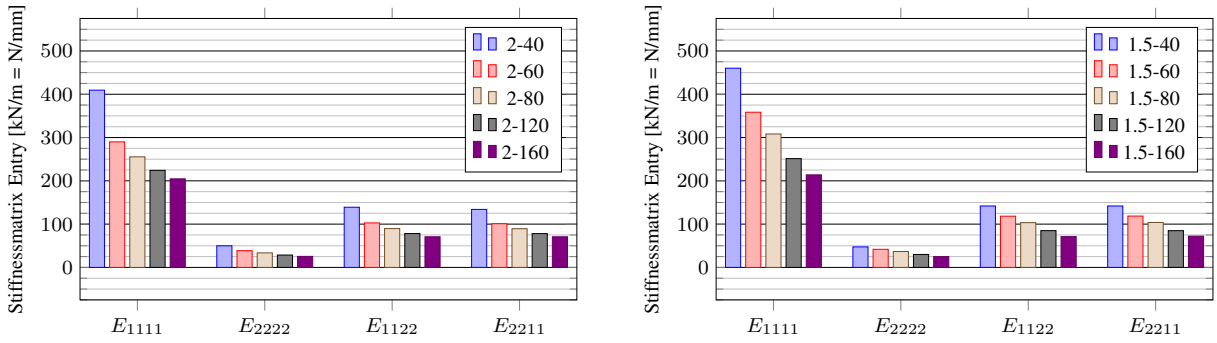

Figure 13: Beam-FEM-BIAX stiffnesses for various mesh types

4.2 Modeling variants of 2-80: higher pretension and higher Young modulus

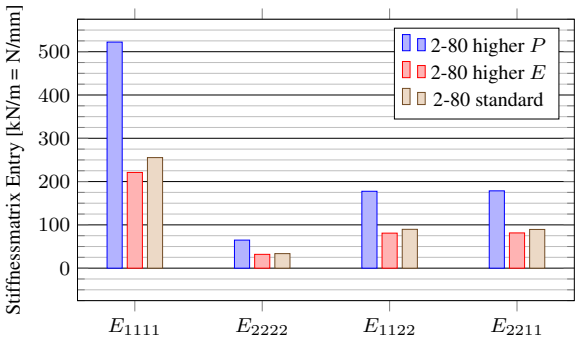

Figure 14: Modeling variants of 2-80

Further modeling variants are performed for type 2-80. As first variant, "higher P", the load P_x is doubled: state 0 is calculated with 160 N per mesh cell, state 1 with 320 N. State 2 is based on the same principle as before.

As second variant, the Young modulus is doubled from $45'000$ to $90'000 N/mm^2$: "higher E". Both "higher P" and "higher E" share same graph with the previously determined 2-80 standard (Fig. 14). It is notable, that "higher P" approx. doubles the stiffness relative to 2-80, however a higher E of the underlining beams again *reduces* the orthotropic stiffness. This is further discussed in section 6.

4.3 Transformation of the Beam-FEM-BIAX results to material properties

Now the Beam-FEM-BIAX results need to be transformed into orthotropic linear-elastic material properties. A slight difference between E_{1122} and E_{2211} can be seen in some types, most significant for 2-40 ($E_{1122} = 139 kN/m$, $E_{2211} = 134 kN/m$) thus violating the required symmetry. The following symmetrization procedure is proposed and applied, in order to maintain the identical interactions value of the asymmetric matrix : $E_{1122,sym} = E_{2211,sym} = \sqrt{(\nu_{12} \cdot \nu_{21})_{asym} \cdot E_{1111} \cdot E_{2222}}$.

The results will again be discussed in section 6, but the high interaction values $\nu_{12} \cdot \nu_{21} > 0.9$ and the low E_1 and E_2 are uncommon compared to membranes[3].

Table 2: Beam-FEM-Stiffness

-	1.5-40	1.5-60	1.5-80	1.5-120	1.5-160	2-40	2-60	2-80	2-120	2-160	*Units*
$E_{1122,asym}$	142	118	103	85	71	139	103	90	78	71	N/mm
$E_{2211,asym}$	142	119	104	85	72	134	101	89	78	71	N/mm
E_{1111}	460	358	308	251	214	409	290	255	224	205	N/mm
E_{2222}	47	42	37	30	25	50	39	34	29	25	N/mm
$E_{1122,sym}$	142	118	104	85	72	136	102	90	78	71	N/mm
$E_{2211,sym}$	142	118	104	85	72	136	102	90	78	71	N/mm
$E1$	35.7	22.5	16.2	10.3	7.8	36.8	21.9	16.4	10.6	8.0	N/mm
$E2$	3.7	2.6	1.9	1.2	0.9	4.5	2.9	2.2	1.3	1.0	N/mm
ν_{12}	2.992	2.837	2.819	2.837	2.873	2.731	2.632	2.668	2.735	2.778	-
ν_{21}	0.308	0.330	0.336	0.338	0.335	0.333	0.351	0.351	0.348	0.346	-
$\nu_{12} \cdot \nu_{21}$	0.922	0.937	0.947	0.959	0.964	0.910	0.924	0.936	0.953	0.961	-

5 SIMPLIFIED BIAX-STIFFNESS OF A TRUSS MODEL

This section illustrates, how a simplified truss-stiffness of the as-installed state of the Webnet can be obtained as alternative hypothesis. Rope bending stiffness is neglected and the rope segments are considered perfectly linear. In the version shown in this paper, also the sleeve geometry is neglected in order to simplify the relations. Using very basic structural engineering concepts, not all intermediate steps are shown.

5.1 X-Direction

The single mesh cell modeled as a truss is first loaded in Y-direction. The geometry and the section stiffness EA_{Truss} is given. The mesh cell and also the membrane element considered equivalent have the same overall dimension and corresponding boundary conditions.

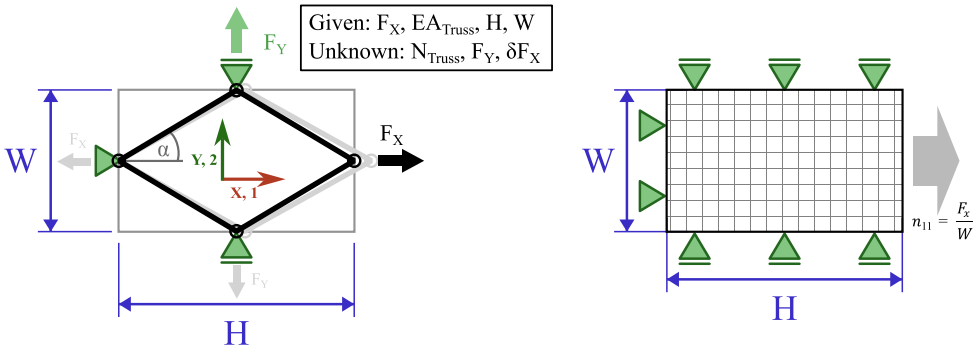

Figure 15: Principle X-direction

The internal angle can also be described as:

$$\cos(\alpha) = \frac{H}{\sqrt{W^2 + H^2}} \tag{6}$$

With nodal equilibrium follows:

$$N_{Truss} = \frac{Fx}{2H} \cdot \sqrt{W^2 + H^2} \qquad (7) \qquad\qquad F_y = \frac{W}{H} \cdot F_x \qquad (8)$$

For δ_{Fx} a virtual load of $'1'$ is applied, with position and direction of F_x. The displacement is then calculated by using the principle of work and energy:

$$\delta_{Fx} = \sum \frac{N_{virt} \cdot N_{Truss} \cdot l}{EA_{Truss}} = \frac{F_x \cdot (W^2 + H^2)^{\frac{3}{2}}}{2 \cdot H^2 \cdot EA_{Truss}} \qquad (9)$$

By distributing the point loads F_x and F_y along W resp. H to obtain n_{11} and n_{22} and under consideration of the general rule $\epsilon = \frac{\Delta l}{l}$, here modified to $\epsilon_{11} = \frac{\delta Fx}{H}$, all the values are available needed to apply equations 3. With $\epsilon_{22} = 0$ as support condition, this

$$\begin{aligned} n_{11} &= E_{1111} \cdot \epsilon_{11} + E_{1122} \cdot \epsilon_{22} \\ n_{22} &= E_{2211} \cdot \epsilon_{11} + E_{2222} \cdot \epsilon_{22} \end{aligned} \qquad (10)$$

simplifies to:

$$\mathbf{E_{1111}} = \frac{\mathbf{2 \cdot H^3 \cdot EA_{Truss}}}{\mathbf{W\,(W^2 + H^2)^{\frac{3}{2}}}} \qquad (11) \qquad\qquad \mathbf{E_{2211}} = \frac{\mathbf{2 \cdot H \cdot W \cdot EA_{Truss}}}{\mathbf{(W^2 + H^2)^{\frac{3}{2}}}} \qquad (12)$$

5.2 Y-Direction

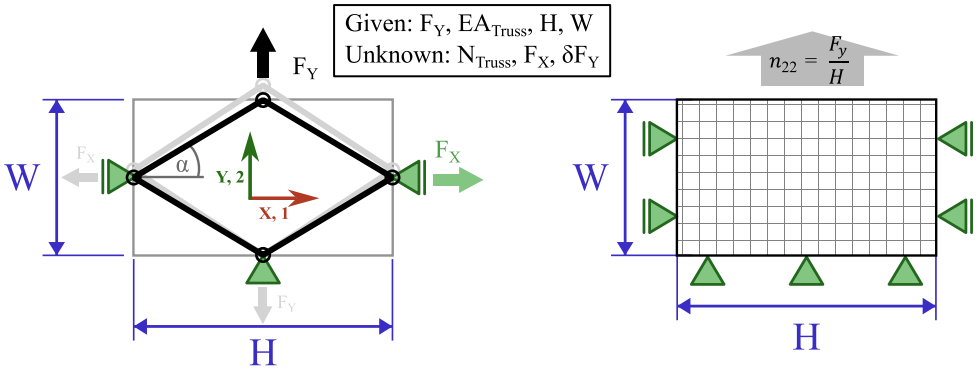

Figure 16: Principle Y-direction

With the same principles as shown in 5.1, it can be determined:

$$N_{Truss} = \frac{F_y}{2W} \cdot \sqrt{W^2 + H^2} \qquad (13) \qquad\qquad F_x = \frac{H}{W} \cdot F_y \qquad (14)$$

$$\delta_{Fy} = \frac{F_y \cdot (W^2 + H^2)^{\frac{3}{2}}}{2 \cdot W^2 \cdot EA_{Truss}} \qquad (15)$$

and further:

$$\mathbf{E_{1122}} = \frac{\mathbf{2 \cdot H \cdot W \cdot EA_{Truss}}}{\mathbf{(W^2 + H^2)^{\frac{3}{2}}}} \quad (16) \qquad \mathbf{E_{2222}} = \frac{\mathbf{2 \cdot W^3 \cdot EA_{Truss}}}{\mathbf{H\,(W^2 + H^2)^{\frac{3}{2}}}} \quad (17)$$

5.3 Complete idealized stiffness matrix

Now the complete stiffness matrix can be built by inserting various exemplary values for EA, W and H:

Table 3: Stiffness based on Truss-Approach

-	Standard	Higher E	Larger Mesh Size	Smaller Diameter	Overstreched v1	Overstreched v2	$Units$
E_{Truss}	9'000	90'000	9'000	9'000	9'000	9'000	N/mm^2
A_{Truss}	1.76	1.76	1.76	0.99	1.76	1.76	mm^2
H	141	141	282	141	135	128	mm
W	80	80	160	80	90	100	mm
E_{1111}	261	2605	130	147	203	154	N/mm
E_{2222}	27	270	14	15	40	58	N/mm
E_{1122}	84	839	42	47	90	95	N/mm
E_{2211}	84	839	42	47	90	95	N/mm
ν_{12}	3.106	3.106	3.106	3.106	2.247	1.628	-
ν_{21}	0.322	0.322	0.322	0.322	0.445	0.614	-
$\nu_{12} \cdot \nu_{21}$	1.000	1.000	1.000	1.000	1.000	1.000	-

It can be seen how the stiffnesses are the proportional to E and A and inverse-proportional to W and H. A variation of the opening angle resp. the effective W/H-ratio, changes the internal ratios. It is apparent, that these values are *not* suitable as stiffness matrices due to the previously defined requirements not being met: interaction value = 1.0 and a $|\mathbf{K}| = 0$. More about the internal stiffness ratios is specified the next chapter, but some internal ratios shall be given as analytical results: $E_{1111}/E_{2222} = H^4/W^4$ and $E_{1111}/E_{1122} = H^2/W^2$ and $\nu_{12} = H^2/W^2$.

5.4 Modified matrix

In order to satisfy $|\mathbf{K}| = E_{1111}E_{2222} - E_{1122}E_{2211} > 0$, the following modification is proposed by introducing the value χ:

$$\begin{bmatrix} n_{11} \\ n_{22} \end{bmatrix} = \begin{bmatrix} \frac{2 \cdot H^3 \cdot EA_{Truss}}{W(W^2+H^2)^{\frac{3}{2}}} & \frac{2 \cdot H \cdot W \cdot EA_{Truss}}{(W^2+H^2)^{\frac{3}{2}}} \\ \frac{2 \cdot H \cdot W \cdot EA_{Truss}}{(W^2+H^2)^{\frac{3}{2}}} & \chi \cdot \frac{2 \cdot W^3 \cdot EA_{Truss}}{H(W^2+H^2)^{\frac{3}{2}}} \end{bmatrix} \cdot \begin{bmatrix} \epsilon_{11} \\ \epsilon_{22} \end{bmatrix} \quad (18)$$

With $\chi > 1.0$, the matrix becomes invertible and thus usable. The justification for the χ will be given in the following section, as it being based on the Beam-FEM-Modeling.

6 COMPARISION AND INTERPRETATION

Now the results of both fundamental hypotheses will be compared and interpreted. Ratios of the stiffness matrix entries are $E_{1111,Beam}/E_{2222,Beam} = 7.5...9.7$ and for standard Truss-type (no χ) $E_{1111,Truss}/E_{2222,Truss} = 9.65$. Further: $E_{1111,Beam}$ / $E_{1122,Beam,sym} = 2.85...3.25$ and $E_{1111,Truss}/E_{1122,Truss} = 3.1$. The similar ratios indicate that both hypotheses are matching.

6.1 Applying the Truss-approach to Beam-FEM results

In order to compare both approaches, E_{Truss} is calibrated, so that $E_{1111,Truss}$ = $E_{1111,Beam}$, (see Tab. 5 for details) and the other "Truss"-values are obtained.

Table 4: Truss and Beam-FEM comparison for 2-80

Type 2-80	[N/mm]	Type 2-80	[N/mm]	Truss/Beam
$E_{1111,Truss}$	255	$E_{1111,Beam}$	255	100%
$E_{2222,Truss}$	26	$E_{2222,Beam}$	34	79%
$E_{1122,Truss}$	82	$E_{1122,Beam,sym}$	90	92%
$E_{2211,Truss}$	82	$E_{2211,Beam,sym}$	90	92%

The Truss-approach seems to underestimate the $E_{1122,Beam,sym}$ moderately and $E_{2222,Beam}$ significantly. That means that to get $|\mathbf{K}_{Truss}| = E_{1111}E_{2222} - E_{1122}E_{2211} > 0$, reducing $E_{1122,Truss}$ and $E_{2211,Truss}$ by a factor < 1 would increase the relative difference between Truss- and Beam-FEM-approach; whereas adding the proposed $\chi > 1$ reduces the difference.

Limiting to E_{1111} and E_{2222} in the next table, it can be seen that $E_{2222,Beam}$ is consistently higher, then what the equivalent truss stiffness would yield. This is an indication, that $E_{2222,Truss}$ is underestimated due to the rope bending not being considered. Thus, the explanation for the correction of the truss-matrix with $\chi > 1$ is given, whereas χ in the table is calculated by $E_{2222,Beam}/E_{2222,Truss}$.

Table 5: Truss and Beam-FEM comparison

-	1.5-40	1.5-60	1.5-80	1.5-120	1.5-160	2-40	2-60	2-80	2-120	2-160	$Units$
E_{Truss}	13'536	16'290	18'911	23'242	26'421	6'777	7'423	8'821	11'687	14'273	N/mm^2
A_{Truss}	0.99	0.99	0.99	0.99	0.99	1.76	1.76	1.76	1.76	1.76	mm^2
H	75	108	141	210.0	280	75	108	141	210	278	mm
W	40	60	80	120	160	40	60	80	120	160	mm
$E_{1111,Truss}$	460	358	308	251	214	409	290	255	224	205	N/mm
$E_{2222,Truss}$	37	35	32	27	23	33	28	26	24	22	N/mm
$E_{1111,Beam}$	460	358	308	251	214	409	290	255	224	205	N/mm
$E_{2222,Beam}$	47	42	37	30	25	50	39	34	29	25	N/mm
χ	1.269	1.204	1.152	1.119	1.094	1.503	1.377	1.270	1.189	1.140	-

The table also shows, how E_{Truss} increases with the mesh size. More about the effective stiffness and the influence of the S-bend is found in the next section.

6.2 Geometric non-linearity

To get more info about the "S-bend-straightening" resp. the behavior under lateral load, the results of section 3.3 are used for further analysis about the geometrical non-linearity. The forces and deflections shown in that chapter can be transformed to an equivalent membrane following the relations illustrated in section 5.1. That means that with $\frac{n_{11}}{\epsilon 11} = E_{1111} = \frac{2 \cdot H^3 \cdot EA_{Truss}}{W(W^2+H^2)^{\frac{3}{2}}}$, first E_{1111} and then with the given A_{Truss}, E_{Truss} can be calculated.

The displacement for an P_x of 100 N and 600 N was taken from Fig. 8 and marked on the E_{1111} curve for both types on Fig. 17 (left). For the displacement at 100 N, the E_{1111} of 1.5-80 is larger than that of 2-80. For the displacement corresponding with P_x = 600 N the ratios are inverted: the 2-80 is stiffer as the 1.5-80, as one would expect of the type with the higher metallic

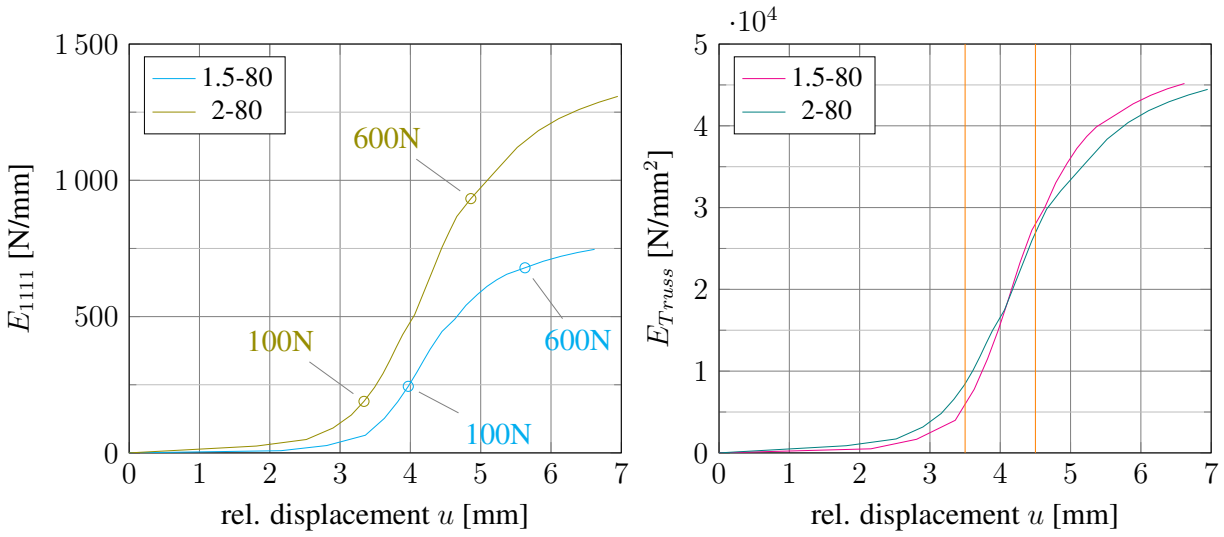

Figure 17: Simulation lateral: orthotropic property (left) and equivalent E_{Truss} (right)

section. The stiffer Beam-FEM-BIAX results of Ø1.5 relative to the Ø2.0 are thus verified for the assumed loads of 80 to 160 N per mesh. The explanation is visualized when looking at Fig. 12: due to the lower rope bending stiffness, the S-bend-straightening of the Ø1.5 is more prominent, thus increasing geometrical stiffness.

On Fig. 17 (right), the corresponding E_{Truss} can be seen: very low ($< 5'000N/mm^2$) for the first three millimeters, the value eventually converges toward the $E_{Beam-FEM} = 45'000N/mm^2$ of the underlining model. The nominal mesh height H of 141 mm is archived by a relative displacement of approx. 4 mm. E_{Truss} is sensitive around that position: a displacement just 1 mm more (i.e. between 3.5. and 4.5 mm, orange lines) increases the corresponding E_{Truss} by approx. factor 3. The softening effect of the S-bend seems to be stronger for smaller mesh types as the results of Tab. 5 indicate: E_{Truss} is increasing with mesh size.

Pretension and as-installed geometry is *the* significant influence of the stiffness. Mesh tension status however can only be measured indirectly and also mesh geometry can not be measured or adjusted to the milimeter exactly in construction practice. The only way to cope with that uncertainty, is by covering a range of stiffnesses during calculations or assume extreme values with a safety margin depending on the structural task.

6.3 Remarks about the interaction

Both Truss- and Beam-approach confirm the "high interaction"-behavior. Visualization of the rational function $E_{1111} = \frac{E_1}{1-\nu_{12}\cdot\nu_{21}}$ is given for various interaction values: for orthotropic textile membranes, the range of $\nu_{12} \cdot \nu_{21}$ is between 0 and 0.45[3], shown as gray area in the graph.

These single-set meshes however, have an interaction value of 0.9 and more (not counting the unsuitable truss interaction of 1.0 at the pole), which increases input sensitivity (orange area). That means that the high interaction does not allow a direct comparison of the materials parameters E_1 and E_2. For example in Tab. 2, the value for E_1 of 2-160 is approx. half of E_1 of 2-80, even though

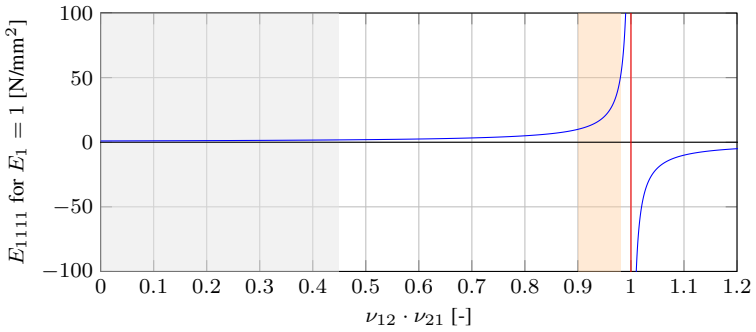

Figure 18: Visualization of the high interaction

E_{1111} is only 20% less. Due to this sensitivity, many digits of ν_{12} must be specified in the material properties and a check of the resulting stiffness matrix is advised.

7 LIMITATIONS AND OUTLOOK

In this paper, it was shown how to obtain the normal stiffness parameters for single-set rope meshes. Using the Truss-Approach, the linear membrane forces can be converted back to cable forces, thus building the basis for failure criteria and allowing design verifications. The S-bend-straightening should be analyzed further, by formulating a curvature dependent tensile stiffness of a bent beam with low bending stiffness.

Further, shear stiffness must be analyzed and incorporated, for example by a Beam-FEM- and by a Truss-Approach as well. Additionally, more single-mesh-tests with higher pretension to better calibrate I and E independently would be advisable and methods to measure in-situ pretension statuses would allow for a refinement of the approaches. The current membrane approach is deemed inaccurate to judge the behavior against point loads or other localized loads. Also energy dissipation considerations may not be approximated with a truss simplification, here the Beam-FEM-Approach could be further developed.

The current surface approaches are however used in many common engineering applications, allowing for global calculations and design checks and by being the basis of the pattering procedure: efficiently creating material saving production plans for completely preassembled mesh areas.

8 CONCLUSIONS

It is possible to formulate the single-set rope meshes as membranes. Both shown hypotheses to obtain the membrane stiffness are valuable: the “Beam-FEM” for verifying the rope bending effect and the effective tensile stiffness due to S-bend-straightening. Due to high variability of possible pretension-conditions resp. initial geometrical stiffness, the engineer must make assumptions about whether to chose a “low” or a “high”-pretension approach. After choosing, the “Truss”-formulas can be used as quick and easy tabular output of mesh configurations. The intrinsic high interaction can be represented with conventional material properties, if input accuracy of the ν is considered and the small E_1 and E_2 are accepted as correct.

8.1 Acknowledgments

A big thank you goes to the board members and the colleagues of Jakob Rope Systems for their support.

REFERENCES

[1] www.dibt.de/en/service/approval-download/detail/z-147-557

[2] Brian Forster, Marijke Mollaert (eds.): European Design Guide for Surface Tensile Structures, ISBN 90 8086 871 X, TensiNet, 2004

[3] Jörg Uhlemann, Natalie Stranghöner, Klaus Saxe: Stiffness Parameters for Architectural Fabrics: An Analysis of Two Determination Procedures. Structural Engineering International 25 (1): 9–19. doi:10.2749/101686614X14043795570291, 2015

[4] Rosemarie Wagner: Bauen mit Seilen und Membranen, ISBN 978-3-410-21719-0, Beuth Verlag GmbH, 2016

[5] Testing by DEKRA Automobil GmbH, PR: 852-03, sample: S17/185, second part, Material type: WEBNET micro 20261-0150-025, 2019

[6] Eurocode 3 - Design of steel structures - Part 1-11: Design of structures with tension components, December 2010

[7] Rosemarie Wagner, Kai Heinlein: Experimentelle Untersuchungen zu Seilnetzen aus hochlegiertem Stahl, Messtechnik im Bauwesen, Ernst und Sohn Special, 2018

[8] Klaus Feyrer: Drahtseile - Bemessung, Betrieb, Sicherheit, 2nd Edition, ISBN 978-3-642-63531-1, Springer, 2000

[9] Konstantin Papailiou: Die Seilbiegung mit einer durch die innere Reibung, die Zugkraft und die Seilkrümmung veränderlichen Biegesteifigkeit, DISS ETH Nr. 11057, 1995